

TECHNICAL EVALUATION OF FUJI AMULET FULL FIELD DIGITAL MAMMOGRAPHY SYSTEM

NHSBSP Equipment Report 0907
November 2009

KC Young, JM Oduko and M Asad
National Coordinating Centre for the Physics of Mammography

Enquiries

Enquiries about this report should be addressed to:

Professor KC Young
National Coordinating Centre for the Physics of Mammography
Medical Physics Department
Royal Surrey County Hospital
Guildford
GU2 7XX

Tel: 01483 406738
Fax: 01483 406742
Email: ken.young@nhs.net

Published by

NHS Cancer Screening Programmes
Fulwood House
Old Fulwood Road
Sheffield
S10 3TH

Tel: 0114 271 1060
Fax: 0114 271 1089
Email: info@cancerscreening.nhs.uk
Website: www.cancerscreening.nhs.uk

© NHS Cancer Screening Programmes 2009

The contents of this document may be copied for use by staff working in the public sector but may not be copied for any other purpose without prior permission from NHS Cancer Screening Programmes. The report is available in PDF format on the NHS Cancer Screening Programmes website.

CONTENTS

ACKNOWLEDGEMENTS	iv
1. INTRODUCTION	1
1.1 Testing procedures and performance standards for digital mammography	1
1.2 Objectives	1
2. METHODS	1
2.1 System tested	1
2.2 Detector response	3
2.3 Dose measurement	3
2.4 Contrast-to-noise ratio	3
2.5 Noise analysis	4
2.6 Image quality measurements	5
3. RESULTS	6
3.1 Detector response	6
3.2 AEC performance	7
3.3 Noise measurements	11
3.4 Image quality measurements	13
3.5 Comparison with other systems	16
4. DISCUSSION	20
5. CONCLUSIONS	20
REFERENCES	21

ACKNOWLEDGEMENTS

The authors are grateful to the staff at Fuji Bedford for their help in evaluating the unit at their site.

1. INTRODUCTION

1.1 Testing procedures and performance standards for digital mammography

This report is one of a series evaluating commercially available digital mammography systems on behalf of the NHS Breast Screening Programme (NHSBSP). The testing methods and standards applied are mainly derived from NHSBSP Equipment Report 0604.¹ This report (which is referred to here as the NHSBSP protocol) uses the same image quality and dose standards as are used in the European protocol.^{2,3} The European protocol was followed where there is a more detailed performance standard, eg for the automatic exposure control (AEC) system.

1.2 Objectives

The purpose of these tests was to determine whether this system meets the main standards in the NHSBSP and European protocols, and to provide performance data for comparison against other manufacturers' products. Where a system meets the minimum standards in the NHSBSP protocol, a separate clinical evaluation is published by the NHSBSP. The final decision on the suitability of a system for use in the NHSBSP depends on a review of both technical and clinical evaluations.

2. METHODS

2.1 System tested

The system uses a dual layer selenium detector with optical switching as illustrated in Figure 1. The tests were conducted at the Fujifilm site in Bedford on the system shown in Figure 2 and described in Table 1.

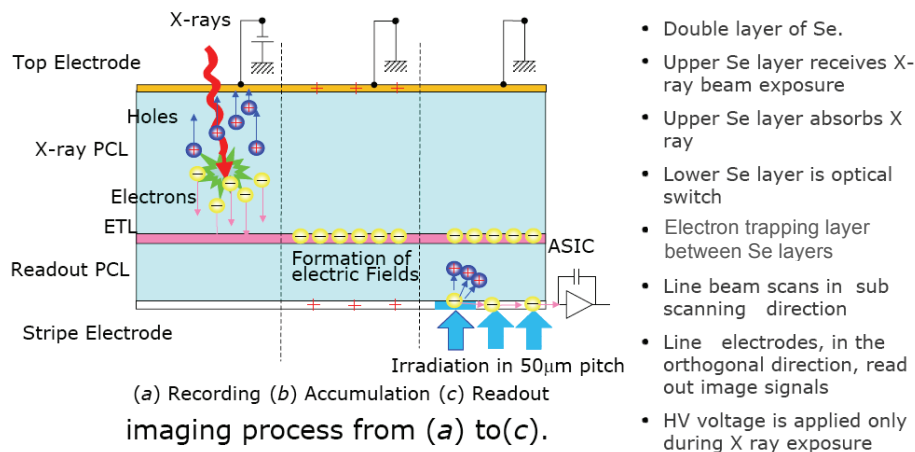


Figure 1 Diagram illustrating operation of the dual selenium layer detector (courtesy of Fuji).



Figure 2 Photograph of Fuji Amulet.

Table 1 System description

Target materials	Molybdenum and tungsten
Added filtration	$30 \pm 5 \mu\text{m}$ molybdenum, $25 \pm 2.5 \mu\text{m}$ rhodium (with Mo tube) $50 \pm 5 \mu\text{m}$ rhodium (with W tube)
Pixel size	$50 \mu\text{m}$ (in detector plane)
Detector area	$177 \times 237 \text{ mm}$
Pixel array	3540×4740
Source to detector distance	650 mm
Software version	FDR-1000AWS Mainsoft T1.0
AEC modes	Normal, small, large

2.2 Detector response

The detector response was measured broadly as described in the NHSBSP protocol. The grid was removed. A phantom of Plexiglas (polymethylmethacrylate, PMMA) with a total thickness of 45 mm was positioned at the tube exit port and exposed using the three target/filter combinations available (Mo/Mo, Mo/Rh and W/Rh) at a tube voltage of 28 kV. An ion chamber was positioned at the surface of the breast support table, and the entrance surface air kerma was measured for a wide range of tube current–time products for each tube voltage and target/filter combination tested. The readings were corrected to the exposed surface above the imaging detector using the inverse square law. It was determined that the imaging detector is at a distance of 650 mm from the tube focus and approximately 17 mm below the protective cover. No correction was made for attenuation by the protective plates above the detector. The images were saved as unprocessed files and transferred to another computer for analysis. A 10 mm square region of interest (ROI) was positioned on the midline and 6 cm from the chest wall edge of each image. The average pixel value and the standard deviation of pixel values within that region were measured. The relationship between average pixel values and the incident air kerma at the exposed surface above the detector was determined and used to linearise the pixel values for subsequent measurements such as contrast-to-noise ratio (CNR) and modulation transfer function (MTF).

2.3 Dose measurement

Doses were measured by using the AEC in each of its three dose modes to expose different thicknesses of PMMA. Each thickness had an area of 18 × 24 cm. Small PMMA spacers were added at the edge of the test object to adjust the total thickness to the equivalent breast thickness. Mean glandular doses (MGDs) were calculated for the equivalent breast thicknesses and the displayed doses recorded. To measure the CNR an aluminium square, 10 × 10 mm and 0.2 mm thick, was placed on top of a 20 mm thick block of PMMA, with one edge on the midline and 6 cm from the chest wall edge. Additional layers of PMMA were placed on top of these to vary the total thickness.

2.4 Contrast-to-noise ratio

The images of the blocks of PMMA obtained during the dose measurement were analysed to obtain the CNRs. Twenty small square ROIs (approximately 2.5 × 2.5 mm) were used to determine the average signal and the standard deviations in the signal within the image of the aluminium square (four ROIs) and the surrounding background (16 ROIs). This is illustrated in Figure 3. Small ROIs are used to minimise distortions due to the heel effect. This is less important than in computed

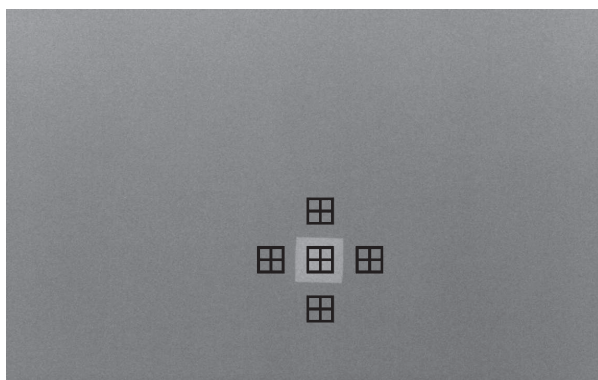


Figure 3 Location and size of ROIs used to determine the CNR.

radiography systems, however, because flat-field correction is applied. The CNR was calculated for each image as defined in the NHSBSP and European protocols. The mean pixel values and fluctuations in those values were corrected for the non-linear detector response. Consequently, the contrast and noise values calculated are for linearised pixel values.

To apply the standards in the European protocol the limiting value for CNR (using 50mm PMMA) was determined according to equation 1. This equation determines the CNR value ($CNR_{limiting\ value}$) that is necessary to achieve the minimum threshold gold thickness for the 0.1 mm detail (ie *threshold gold* $_{limiting\ value} = 1.68\ \mu\text{m}$, which is equivalent to *threshold contrast* $_{limiting\ value} = 23.0\%$ using 28 kV Mo/Mo). Threshold contrasts were calculated as described in the European protocol and used in equation 1.

$$CNR_{limiting\ value} = CNR_{measured} \times \frac{TC_{measured}}{TC_{limiting\ value}} \quad (1)$$

The relative CNR was then calculated according to equation 2 and compared with the limiting values provided for relative CNR shown in Table 1. The minimum CNR required to meet this criterion was then calculated.

$$Relative\ CNR = CNR_{measured} / CNR_{limiting\ value} \quad (2)$$

Table 1 Limiting values for relative CNR

Thickness of PMMA (mm)	Equivalent breast thickness (mm)	Limiting values for relative CNR (%) in European protocol
20	21	> 115
30	32	> 110
40	45	> 105
45	53	> 103
50	60	> 100
60	75	> 95
70	90	> 90

2.5 Noise analysis

The images and ROI produced in the measurements of detector response were used to analyse the image noise. The average standard deviations of the pixel values in the ROI for each image were used to investigate the relationship between the dose to the detector and image noise. It was assumed that this noise comprises three components, electronic noise, structural noise and quantum noise, and that their relationship is as shown in equation 3. This method of analysis has been described elsewhere.⁵

$$\sigma_p = \sqrt{k_e^2 + k_q^2 p + k_s^2 p^2} \quad (3)$$

where σ_p is the standard deviation in pixel values within an ROI with a uniform exposure and a mean pixel value p , and k_e , k_q and k_s are the coefficients determining the amount of electronic, quantum and structural noise, respectively, in a pixel with a value p . For simplicity the noise is generally presented here as relative noise, defined as in equation 4.

$$\text{Relative noise} = \frac{\sigma_p}{p} \quad (4)$$

The variation in relative noise with mean pixel value was evaluated and fitted using equation 3, and non-linear regression was then used to determine the best fit for the constants and their asymptotic confidence limits (using GraphPad Prism Version 5.00 for Windows, GraphPad Software, San Diego, CA, USA, www.graphpad.com). This established whether the experimental measurements of the noise fitted this equation, and the relative proportions of the different noise components. In fact the relationship between noise and pixel values has been found empirically to be approximated by a simple power relationship, as shown in equation 5.

$$\frac{\sigma_p}{p} = k_t p^{-n} \quad (5)$$

where k_t is a constant. If the noise were purely quantum noise, the value of n would be 0.5. However the presence of electronic and structural noise means that n can be slightly higher or lower than 0.5.

2.6 Image quality measurements

Contrast-detail measurements were made using the CDMAM phantom (version 3.4, UMC St Radboud, Nijmegen University, Netherlands). The phantom was positioned with a 20 mm thickness of PMMA above and below, to give a total attenuation approximately equivalent to 50 mm of PMMA or 60 mm thickness of typical breast tissue. An exposure was made with the kV target/filter combinations and mAs chosen to match as closely as possible that selected by the AEC when imaging a 5 cm thickness of PMMA. This procedure was repeated with small adjustments to the phantom position to obtain a representative sample of 16 images at this dose level. Unprocessed images were transferred to disk for subsequent analysis off-site. Further images of the test phantom were then obtained at other dose levels by manually selecting higher and lower mAs values with the same beam quality.

An automatic method of reading the CDMAM images was used.⁴⁻⁶ The threshold gold thickness for a typical human observer was predicted using equation 6.

$$TC_{\text{predicted}} = r TC_{\text{auto}} \quad (6)$$

where $TC_{\text{predicted}}$ is the predicted threshold contrast for a typical observer and TC_{auto} is the threshold contrast measured using an automated procedure with CDMAM images. Contrasts were calculated from gold thickness for a nominal tube voltage of 28 kV and a Mo/Mo target/filter combination as described in the European protocol. r is the average ratio between human and automatic threshold contrast determined experimentally, with the values shown in Table 2.⁴

Table 2 Values of r used to predict threshold contrast

Diameter of gold disc (mm)	Average ratio of human to automatically measured threshold contrast (r)
0.08	1.40
0.10	1.50
0.13	1.60
0.16	1.68
0.20	1.75
0.25	1.82
0.31	1.88
0.40	1.94
0.50	1.98
0.63	2.01
0.80	2.06
1.00	2.11

The main advantage of automatic reading is that it has the potential for eliminating observer error, which is a significant problem when using human observers. However it should be noted that the official protocols are currently based on human reading.

The predicted threshold gold thickness for each detail diameter at each dose level was fitted with a curve, as described in the NHSBSP protocol. The confidence limits for the predicted threshold gold thicknesses have been previously determined by a resampling method using a large set of images. The threshold contrasts quoted in the tables of results are derived from the fitted curves, as this has been found to improve accuracy.⁴

The expected relationship between threshold contrast and dose is shown in equation 7.

$$\text{Threshold contrast} = \lambda D^{-n} \quad (7)$$

D represents the MGD for a 60mm thick standard breast equivalent to the test phantom configuration used for the image quality measurement. λ is a constant to be fitted. It is assumed that a similar equation applies when using threshold gold thickness rather than contrast. This equation was plotted with the experimental data for each detail size, from 0.1 to 1.0mm. The value of n resulting in the best fit with the experimental data was determined.

3. RESULTS

3.1 Detector response

The detector was found to have a logarithmic response for each of the target/filter combinations, as shown in Figure 4. The exposures selected by the AEC resulted in average pixel values in the range 1800–2100, depending on the mode selected and the simulated breast thickness. A standard value of 2050 was chosen to determine the reference entrance air kerma, which was 105.3 μGy using 28 kV W/Rh.

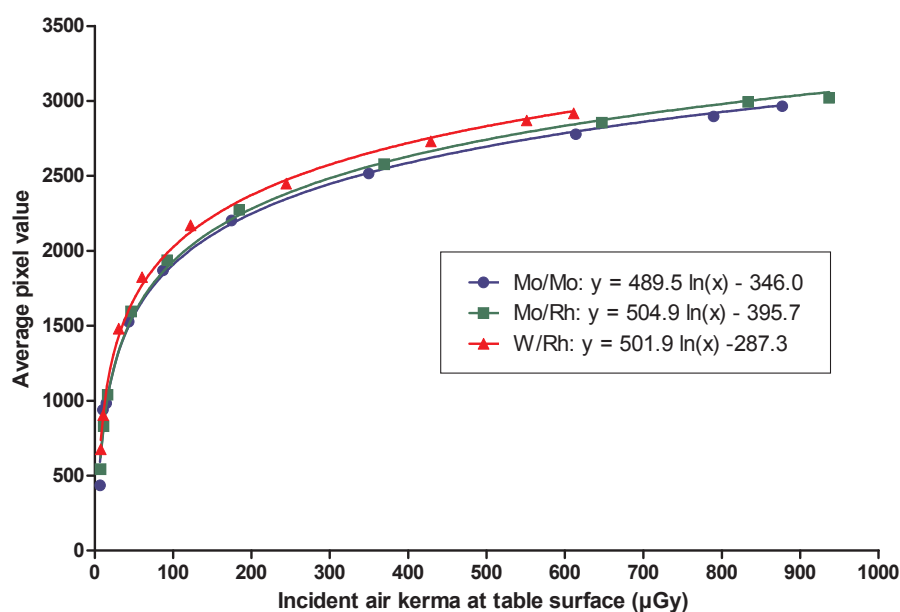


Figure 4 Detector response.

3.2 AEC performance

3.2.1 Dose

The MGDs for breasts simulated with PMMA exposed under AEC control are shown in Table 3 and Figure 5 for the three AEC modes available. At all thicknesses the dose was below the remedial level in the NHSBSP protocol, which is the same as the maximum acceptable level in the European protocol.

Table 3a Mean glandular dose for simulated breasts (AEC in normal mode)

PMMA thickness (mm)	Equivalent breast thickness (mm)	kV	Target	Filter	mAs	MGD (mGy)	Displayed dose (mGy)	NHSBSP remedial level (mGy)
20	21	26	W	Rh	36	0.55	0.52	> 1.0
30	32	27	W	Rh	58	0.80	0.73	> 1.5
40	45	28	W	Rh	77	0.97	0.85	> 2.0
45	53	29	W	Rh	86	1.12	0.93	> 2.5
50	60	30	W	Rh	93	1.24	1.02	> 3.0
60	75	31	W	Rh	138	1.78	1.48	> 4.5
70	90	32	W	Rh	196	2.44	1.85	> 6.5

Table 3b Mean glandular dose for simulated breasts (AEC in large mode)

PMMA thickness (mm)	Equivalent breast thickness (mm)	kV	Target	Filter	mAs	MGD (mGy)	Displayed dose (mGy)	NHSBSP remedial level (mGy)
20	21	27	Mo	Mo	20	0.79	0.73	> 1.0
30	32	28	Mo	Mo	33	1.13	1.00	> 1.5
40	45	28	Mo	Rh	59	1.43	1.26	> 2.0
45	53	29	Mo	Rh	70	1.79	1.49	> 2.5
50	60	30	Mo	Rh	83	2.23	1.83	> 3.0
60	75	29	W	Rh	240	2.54	1.94	> 4.5
70	90	30	W	Rh	358	3.69	2.79	> 6.5

Table 3c Mean glandular dose for simulated breasts (AEC in small mode)

PMMA thickness (mm)	Equivalent breast thickness (mm)	kV	Target	Filter	mAs	MGD (mGy)	Displayed dose (mGy)	NHSBSP remedial level (mGy)
20	21	26	W	Rh	24	0.37	0.35	> 1.0
30	32	27	W	Rh	38	0.52	0.48	> 1.5
40	45	28	W	Rh	50	0.63	0.55	> 2.0
45	53	29	W	Rh	55	0.72	0.60	> 2.5
50	60	30	W	Rh	62	0.82	0.68	> 3.0
60	75	31	W	Rh	90	1.16	0.97	> 4.5
70	90	32	W	Rh	127	1.58	1.29	> 6.5

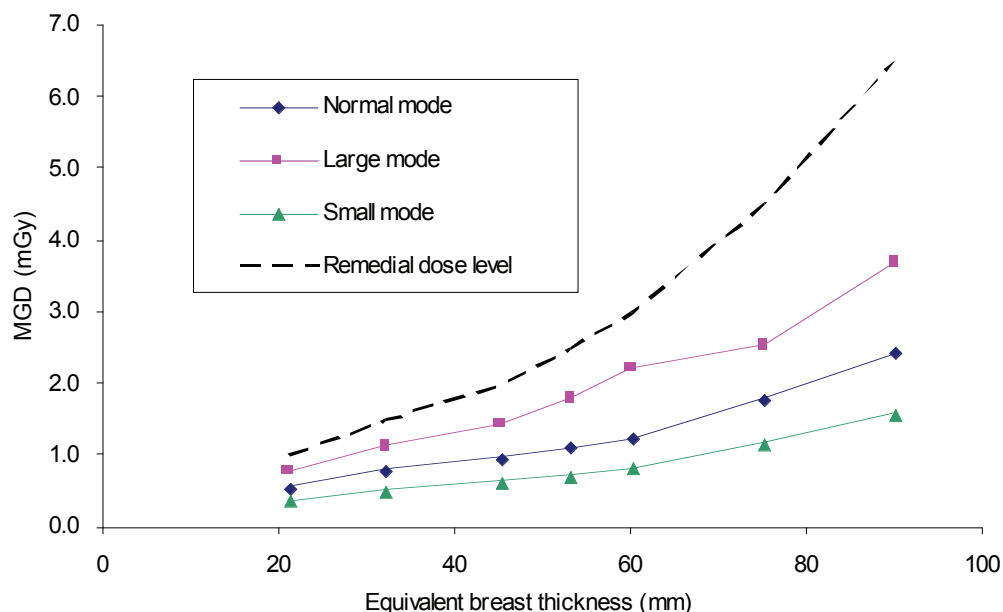


Figure 5 MGD for different thicknesses of simulated breasts using the three AEC modes.

3.2.2 CNR

The results of the contrast and CNR measurements are shown in Table 4 and Figure 6. The CNR required to meet the minimum acceptable and achievable image quality (IQ) standards at the 60 mm breast thickness have been calculated and are shown in Table 4 and Figure 6. The CNR required at each thickness to meet the limiting values for CNR in the European protocol is also shown.

Table 4a Contrast and CNR measurements using AEC (normal mode)

Equivalent breast thickness (mm)	kV Target/ filter	mAs	Back-ground pixel value*	% contrast for 0.2mm		CNR at minimum acceptable IQ	CNR at achievable IQ	CNR to meet European limiting value	European limiting values for relative CNR
				AI	Measured CNR				
21	26 W/Rh	36	146	15.6	12.4	5.25	7.64	6.04	>115
32	27 W/Rh	58	155	14.3	11.7	5.25	7.64	5.77	>110
45	28 W/Rh	77	132	13.5	10.0	5.25	7.64	5.51	>105
53	29 W/Rh	86	127	13.1	9.2	5.25	7.64	5.41	>103
60	30 W/Rh	93	119	12.3	8.4	5.25	7.64	5.25	>100
75	31 W/Rh	138	119	11.3	7.6	5.25	7.64	4.99	>95
90	32 W/Rh	196	126	9.9	6.5	5.25	7.64	4.72	>90

*Linearised with respect to the dose to the detector.

Table 4b Contrast and CNR measurements using AEC (large mode)

Equivalent breast thickness (mm)	kV Target/ filter	mAs	Back-ground pixel value*	% contrast for 0.2mm		CNR at minimum acceptable IQ	CNR at achievable IQ	CNR to meet European limiting value	European limiting values for relative CNR
				AI	Measured CNR				
21	27 Mo/Mo	20	122	19.7	15.1	5.25	7.64	6.04	>115
32	28 Mo/Mo	33	121	17.6	13.0	5.25	7.64	5.77	>110
45	28 Mo/Rh	59	128	15.1	11.3	5.25	7.64	5.51	>105
53	29 Mo/ Rh	70	134	14.1	10.5	5.25	7.64	5.41	>103
60	30 Mo/Rh	83	142	13.0	9.9	5.25	7.64	5.25	>100
75	30 W/Rh	240	147	12.2	9.4	5.25	7.64	4.99	>95
90	30 W/Rh	358	154	11.2	8.6	5.25	7.64	4.72	>90

*Linearised with respect to the dose to the detector.

Table 4c Contrast and CNR measurements using AEC (small mode)

Equivalent breast thickness (mm)	kV Target/ filter	mAs	Back-ground pixel value*	% contrast for 0.2mm Al	Measured CNR	CNR at minimum acceptable IQ	CNR at achievable IQ	CNR to meet European limiting value	European limiting values for relative CNR
21	26 W/Rh	24	101	15.8	10.4	5.25	7.64	6.04	>115
32	27 W/Rh	38	101	14.3	9.4	5.25	7.64	5.77	>110
45	28 W/Rh	50	85	13.9	8.0	5.25	7.64	5.51	>105
53	29 W/Rh	55	80	13.4	7.5	5.25	7.64	5.41	>103
60	30 W/Rh	62	79	12.7	7.0	5.25	7.64	5.25	>100
75	31 W/Rh	90	79	11.4	6.1	5.25	7.64	4.99	>95
90	32 W/Rh	127	81	10.1	5.4	5.25	7.64	4.72	>90

*Linearised with respect to the dose to the detector.

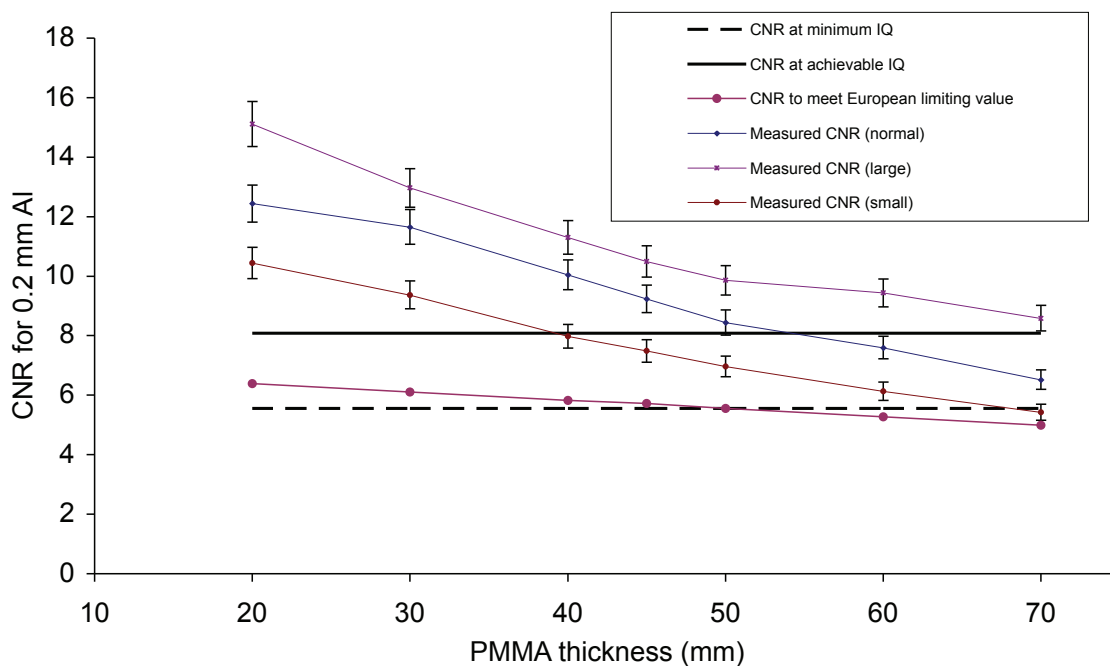


Figure 6 Measured CNR compared with the limiting values in the European protocol for the system. (Error bars indicate 95% confidence limits.)

3.3 Noise measurements

The variation in noise with dose was analysed by plotting the standard deviation in pixel values against the detector entrance air kerma, as shown in Figure 7. Owing to the presence of electronic and structural noise, the fitted power curve does not form a straight line; this is analysed further in subsequent graphs.

In Figure 8 the relative noise is plotted against the incident air kerma using 30 kV W/Rh. Curves of the form described in equation 5 have been fitted to the lower, middle and upper detector dose levels with coefficients of 1.07, 0.58 and 0.44 respectively. A value for n of 0.5 would be expected if quantum noise alone were present. Coefficient values above 0.5 at lower dose levels indicate the presence of electronic noise.

Figure 9 is an alternative way of presenting the data and shows the relative noise at different incident air kerma. The estimated relative contributions of electronic, structural and quantum noise are shown and the quadratic sum of these contributions is fitted to the measured noise using equation 3.

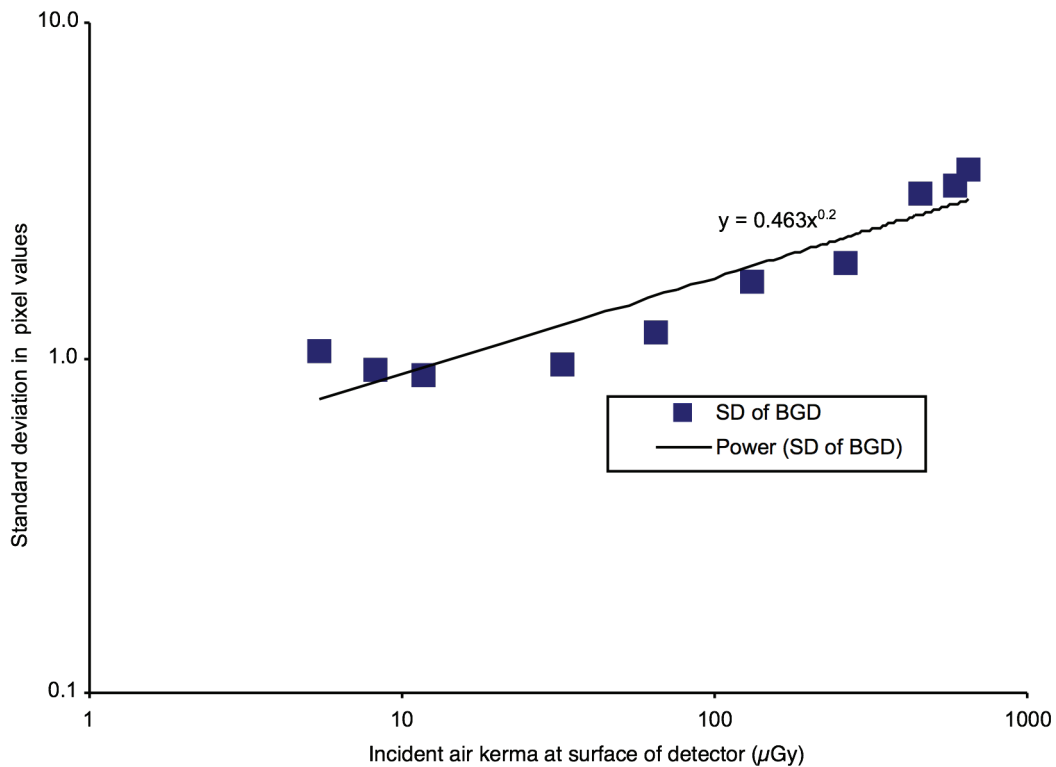


Figure 7 Standard deviation of pixel values versus incident air kerma at detector.

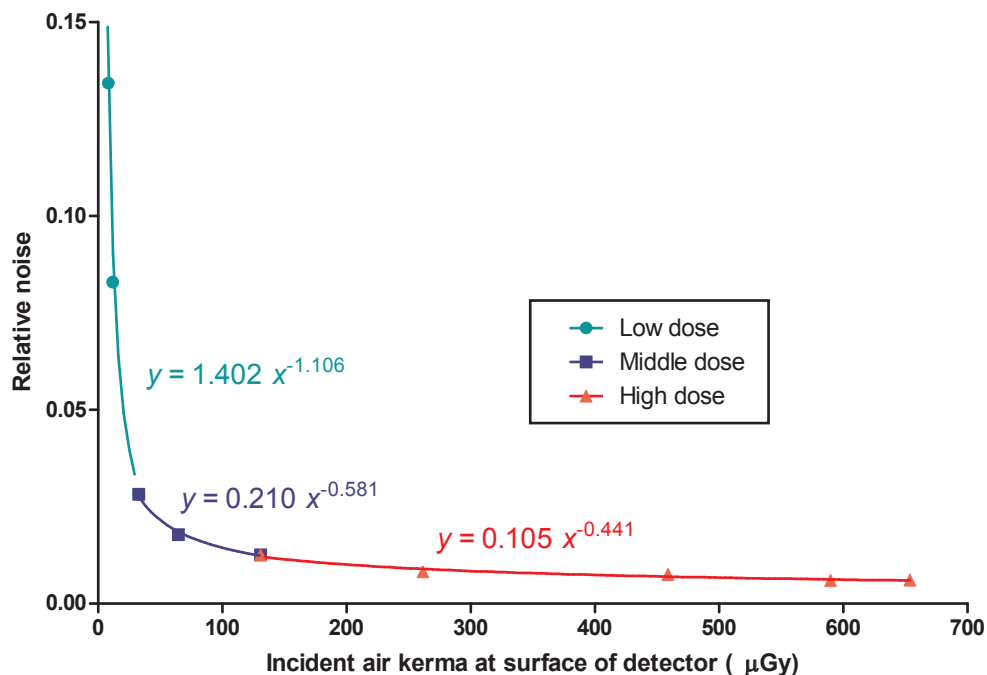


Figure 8 Relative noise at different incident air kerma.

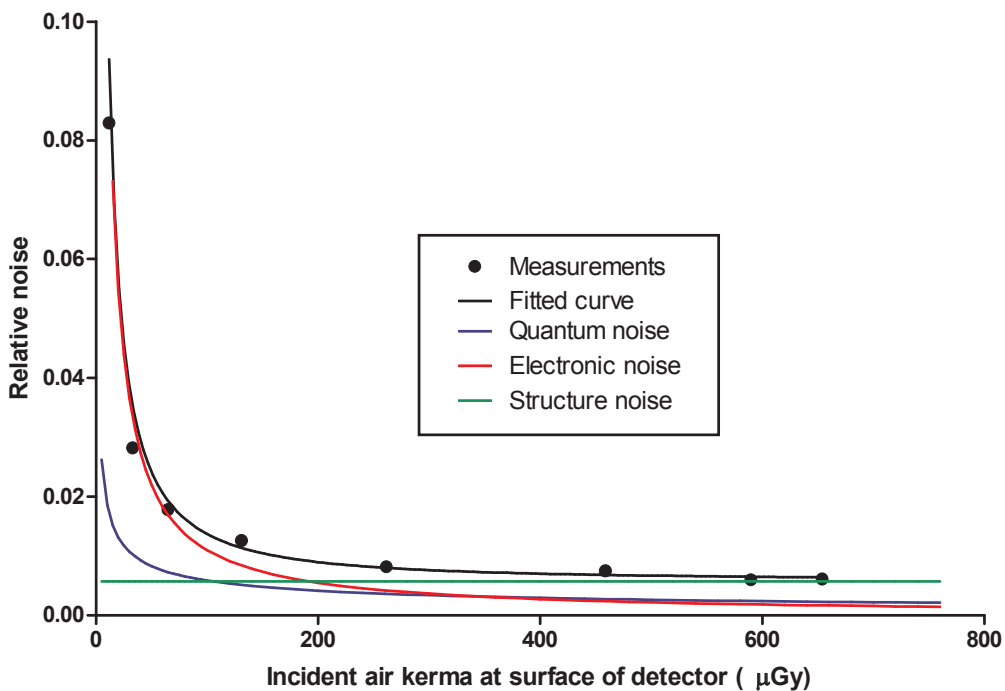


Figure 9 Relative noise and noise components at different incident air kerma using W/Rh target/filter combination.

3.4 Image quality measurements

The exposures of the image quality phantom were based on the selections by the AEC in normal mode for a 5 cm thickness of PMMA. This resulted in the manual selection of 30 kV W/Rh and 90 mAs and an MGD of 1.16 mGy to an equivalent breast (60 mm thick). Subsequent image quality measurements were made at approximately one-quarter, one-half, double and quadruple this dose by manual selection of the mAs, as shown in Table 5.

Table 5 Images acquired for image quality measurement

Exposure mode	kV target/filter	Tube loading (mAs)	Mean glandular dose to equivalent breasts 60 mm thick (mGy)	Number of CDMAM images acquired and analysed
Manual	30 W/Rh	22	0.28	16
Manual	30 W/Rh	45	0.58	16
AEC (normal)	30 W/Rh	90	1.16	16
Manual	30 W/Rh	180	2.31	16
Manual	30 W/Rh	360	4.63	16

The contrast-detail curves at the five dose levels are shown in Figure 10. The threshold gold thicknesses for different diameters and the five different dose levels for this system are shown in Table 6, along with the minimum and achievable threshold values from the NHSBSP protocol (which are the same as the European protocol). The data in Table 6 are taken from the fitted curves rather than the raw data.

In Figure 11 the measured threshold gold thicknesses are plotted against the MGD for an equivalent breast for the 0.1 and 0.25 mm detail sizes. This shows how the threshold gold thickness reduced as the dose was increased. Fitted curves (such as those shown in Figure 11) were used to determine the doses required to meet the minimum acceptable and achievable image quality levels for detail sizes from 0.1 to 1.0 mm. The results are shown in Figure 12.

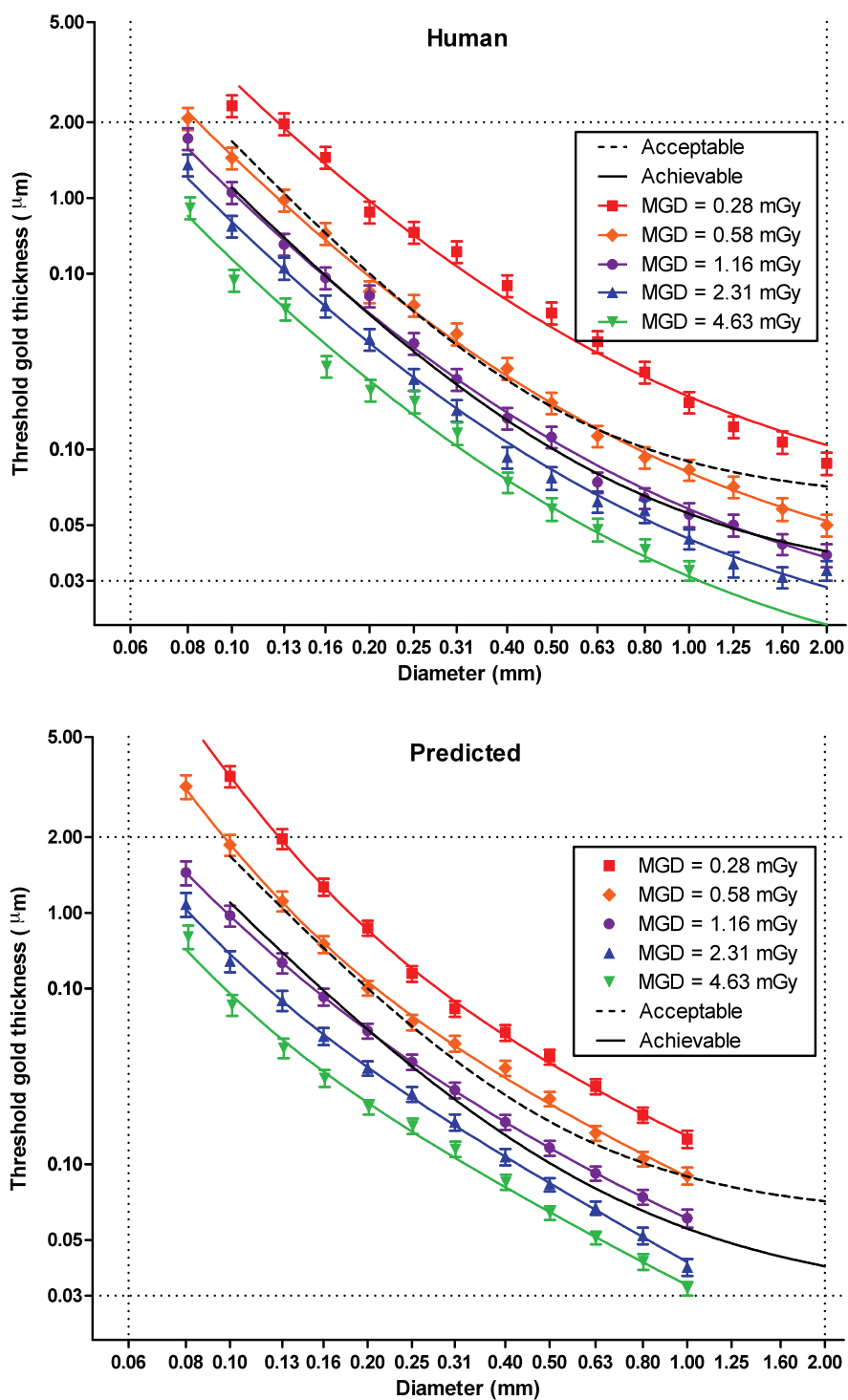


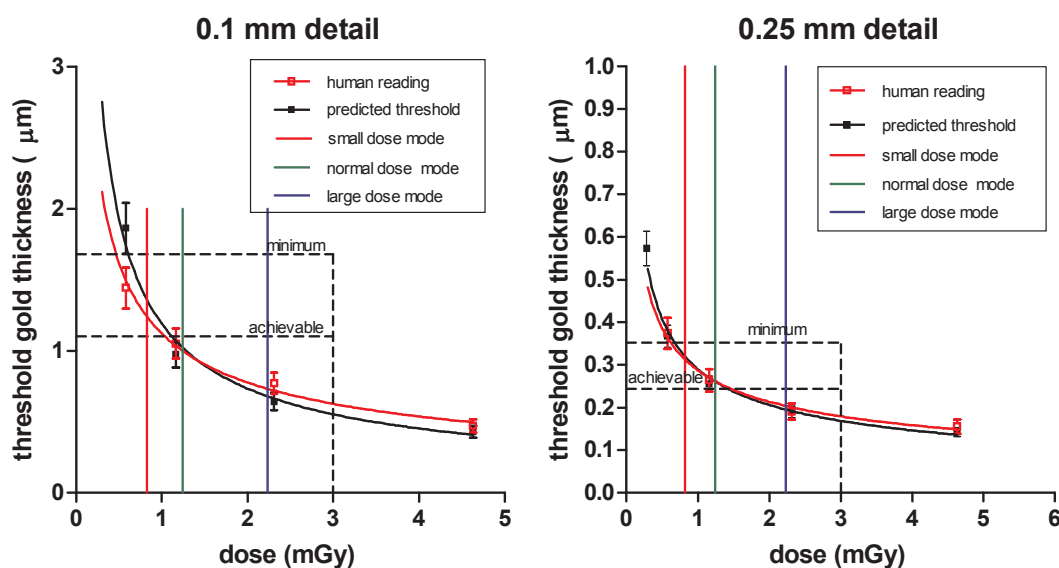
Figure 10 Contrast-detail curves for the system for five different doses at 30 kV W/Rh using human and predicted results from automated reading. The 1.16 mGy dose corresponds to the AEC selection in normal mode. (Error bars indicate 95% confidence limits.)

Table 6a Average threshold gold thicknesses for different detail diameters for five different doses using 30kV W/Rh and human data. (Data are interpolated using curve fits.)

Diameter (mm)	Threshold gold thickness (μm)						
	Acceptable value	Achievable value	MGD=0.28 mGy	MGD=0.58 mGy	MGD=1.16 mGy	MGD=2.31 mGy	MGD=4.63 mGy
0.1	1.680	1.100	2.753 ± 0.275	1.485 ± 0.149	1.142 ± 0.114	0.902 ± 0.090	0.631 ± 0.063
0.25	0.352	0.244	0.742 ± 0.074	0.358 ± 0.036	0.253 ± 0.025	0.186 ± 0.019	0.132 ± 0.013
0.5	0.150	0.103	0.331 ± 0.033	0.155 ± 0.015	0.106 ± 0.011	0.080 ± 0.008	0.062 ± 0.006
1	0.091	0.056	0.163 ± 0.016	0.080 ± 0.008	0.056 ± 0.006	0.044 ± 0.004	0.034 ± 0.003

Table 6b Average threshold gold thicknesses for different detail diameters for five different doses using 30kV W/Rh and automatically predicted data. (Data are interpolated using curve fits.)

Diameter (mm)	Threshold gold thickness (μm)						
	Acceptable value	Achievable value	MGD=0.28 mGy	MGD=0.58 mGy	MGD=1.16 mGy	MGD=2.31 mGy	MGD=4.63 mGy
0.1	1.680	1.100	3.460 ± 0.516	1.843 ± 0.185	0.994 ± 0.100	0.656 ± 0.066	0.433 ± 0.065
0.25	0.352	0.244	0.600 ± 0.049	0.387 ± 0.019	0.260 ± 0.013	0.185 ± 0.009	0.134 ± 0.011
0.5	0.150	0.103	0.253 ± 0.021	0.173 ± 0.009	0.118 ± 0.006	0.081 ± 0.004	0.063 ± 0.005
1	0.091	0.056	0.129 ± 0.015	0.091 ± 0.007	0.061 ± 0.004	0.042 ± 0.003	0.035 ± 0.004


Figure 11 Threshold gold thickness at different doses predicted from automatic reading of CDMAM images. (Error bars indicate 95% confidence limits.) The doses selected for a 5 cm thickness of PMMA using the three AEC dose modes are shown by the coloured vertical lines.

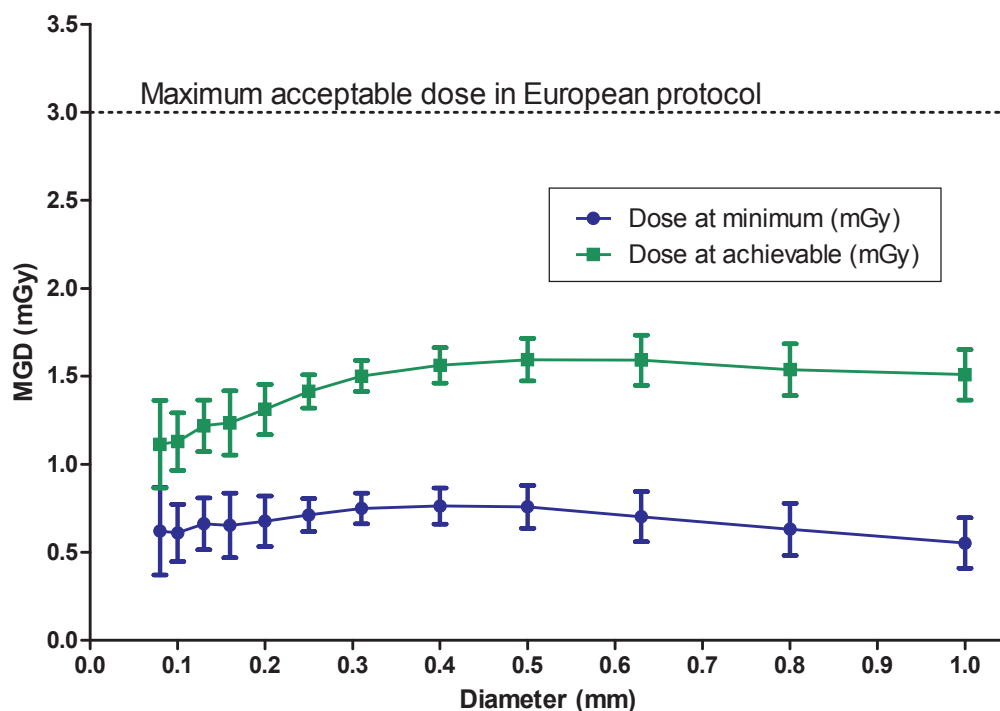


Figure 12 The MGD calculated to be necessary to reach the achievable and minimum acceptable image quality levels at different detail sizes using 30 kV W/Rh for an equivalent breast 60 mm thick. Based on predicted threshold gold thicknesses.

3.5 Comparison with other systems

The MGDs to reach the minimum and achievable image quality standards in the NHSBSP protocol have been estimated from the curves shown in Figure 11. (The error in estimating these doses depends on the accuracy of the curve fitting procedure; pooled data for several systems have been used here to estimate the 95% confidence limits of approximately 20%.) These doses are shown against similar data for other models of digital mammography system in Tables 7 and 8 and Figures 13 to 16. The data for the other systems have been determined in the same way as described in this report and the results published elsewhere.⁷⁻¹⁶ The data for film-screens represent an average value determined using a variety of modern film-screen systems.

Table 7 The MGD for different systems to reach the minimum threshold gold thickness for 0.1 and 0.25 mm details

System	MGD (mGy) for 0.1 mm		MGD (mGy) for 0.25 mm	
	Human	Predicted	Human	Predicted
Sectra MDM-L30	0.41		0.41	0.42
Siemens Novation*	0.54	0.59	0.47	0.67
Fuji Amulet	0.62	0.67	0.74	0.71
Hologic Selenia (W)	0.58	0.70	0.65	0.86
Hologic Selenia (Mo)	0.85	0.55	0.80	0.53
GE Essential	0.6	0.49	0.50	0.49
GE DS	1.01	0.82	0.87	0.83
IMS Giotto (W)	1.07	1.38	0.91	1.17
Film screen	1.17	1.30	1.07	1.36
Konica Minolta (CP-1M)	1.60	1.47	1.12	0.99
Fuji Profect CR	1.67	1.78	1.45	1.35
Agfa CR 85-X (MM3.0)	2.00	1.94	0.86	1.42
Kodak CR (EHR-M2)	2.29	2.34	1.45	1.80

*Mean of measurements for two systems in NHSBSP Equipment Report 0710.¹²

Table 8 The MGD for different systems to reach the achievable threshold gold thickness for 0.1 and 0.25 mm details

System	MGD (mGy) for 0.1 mm		MGD (mGy) for 0.25 mm	
	Human	Predicted	Human	Predicted
Sectra MDM-L30	1.09	2.04	0.95	0.97
Siemens Novation*	1.30	2.26	1.00	1.37
Fuji Amulet	1.40	1.13	1.50	1.41
Hologic Selenia (W)	1.66	1.37	1.61	1.48
Hologic Selenia (Mo)	1.84	1.19	1.68	1.12
GE Essential	1.57	1.13	1.14	1.03
GE DS	2.35	1.57	1.80	1.87
IMS Giotto (W)	2.33	2.73	1.77	2.11
Film screen	2.48	3.03	2.19	2.83
Konica Minolta (CP-1M)	4.53	3.45	2.73	2.08
Fuji Profect CR	4.26	3.29	3.52	2.65
Agfa CR 85-X (MM3.0)	5.03	4.88	2.20	3.15
Kodak CR (EHR-M2)	5.34	5.45	3.03	3.74

*Mean of measurements for two systems in NHSBSP Equipment Report 0710.¹²

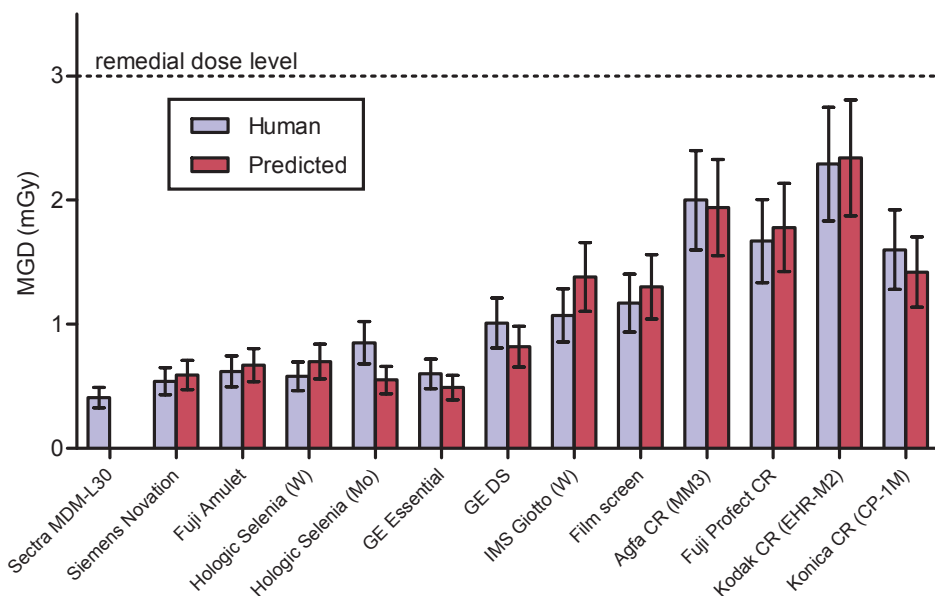


Figure 13 Dose to reach minimum acceptable image quality standard for 0.1 mm detail. (Error bars indicate 95% confidence limits.)

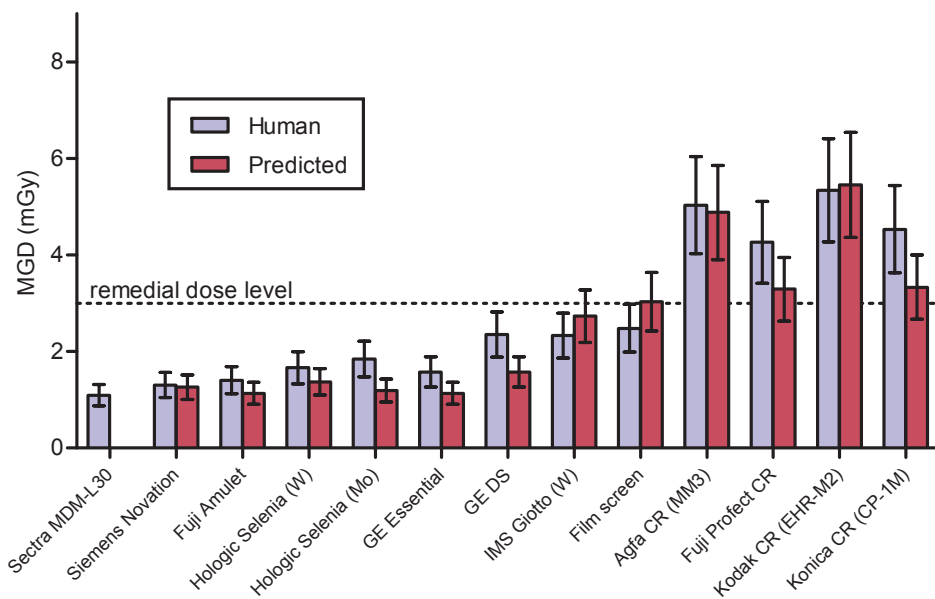


Figure 14 Dose to reach achievable image quality standard for 0.1 mm detail. (Error bars indicate 95% confidence limits.)

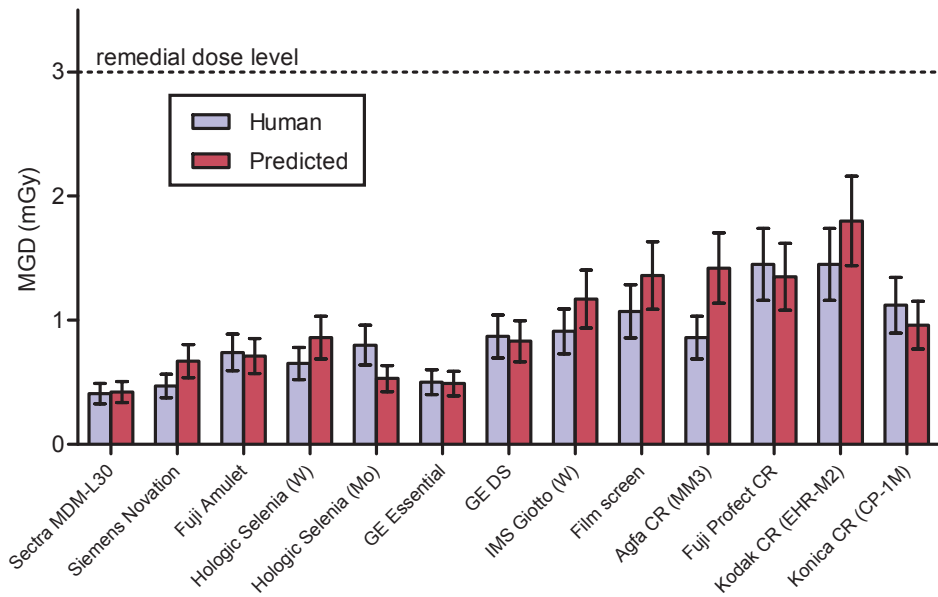


Figure 15 Dose to reach minimum acceptable image quality standard for 0.25 mm detail (Error bars indicate 95% confidence limits.)

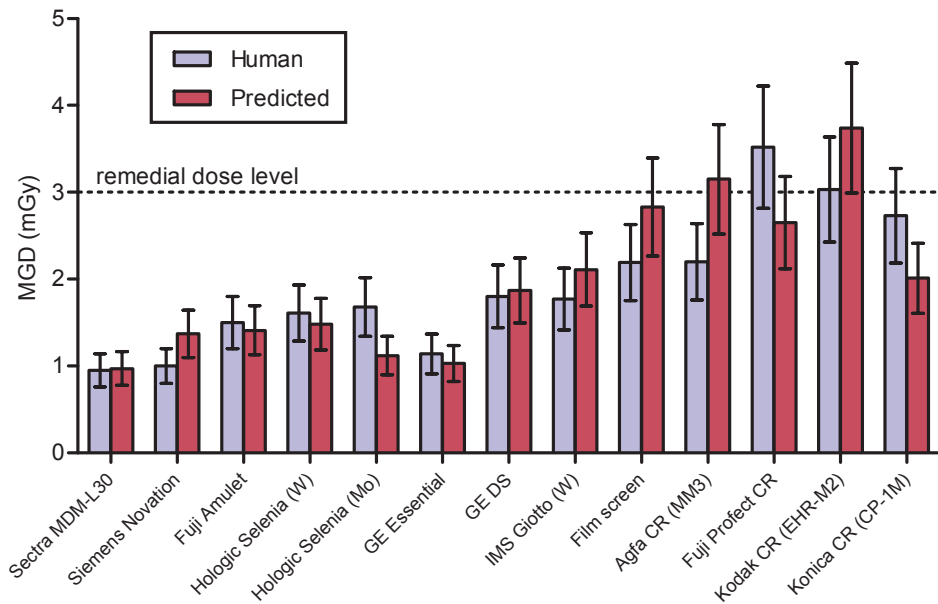


Figure 16 Dose to reach achievable image quality standard for 0.25 mm detail. (Error bars indicate 95% confidence limits.)

4. DISCUSSION

The detector response was found to be logarithmic. This is exceptional for a digital radiography (DR) system but typical for a computed radiography (CR) system. The noise analysis suggests that there are substantial amounts of electronic and structural noise even at the exposures used clinically. This is something that merits further investigation. In all three dose modes the AEC resulted in doses to simulated breasts that were well below the limits in the NHSBSP protocol. The doses for the standard breast simulated with 45 mm of PMMA in the three modes were 0.72, 1.12 and 1.79 mGy. At this thickness an upper limit of 2.5 mGy is applied by the NHSBSP. The doses calculated and displayed by the system itself were higher than those calculated by us. The reason for these differences is not clear.

The three AEC modes resulted in background raw pixel values that varied between 1800 and 2100 depending on the thickness and mode used. In the normal and small dose modes the AEC chose the W/Rh target/filter combination for all simulated breast thicknesses with a tube voltage in the range 26–32 kV. In the large dose mode lower energy spectra were selected by using Mo/Mo and Mo/Rh target/filter combinations for the lower and average breast thicknesses. The net result of these choices was that the CNR values were relatively high for thinner breasts but dropped steeply with increasing breast thickness, as shown in Figure 6. All three AEC modes exceeded the minimum requirements in the European protocol. However the CNR values seemed much higher than necessary for the thinner breasts, while falling well below that necessary to reach the achievable level of image quality for the largest simulated thicknesses. At all settings the minimum acceptable CNR value was met or exceeded.

The image quality measurements indicated that for the standard thickness tested (equivalent to 50 mm thickness of PMMA or 60 mm of typical breast) the image quality was close to the achievable level in normal mode. In this mode the AEC selected a dose of 1.16 mGy using 30 kV W/Rh. A dose of approximately 0.67 ± 0.15 mGy was calculated to be necessary to reach the minimum image quality level for this equivalent breast thickness at the 0.1 mm detail size. A dose of approximately 1.21 ± 0.15 mGy was calculated to be necessary to reach the achievable image quality level for this equivalent breast thickness at the 0.1 mm detail size.

The doses required to reach the acceptable and achievable image quality levels are similar to those reported by the authors for other DR systems using selenium detectors and are broadly similar to other DR systems.

5. CONCLUSIONS

This system is capable of producing excellent image quality with a relatively low radiation dose. As currently set up the AEC will be satisfactory for most types of breast in all three AEC modes. It is expected that the normal AEC mode will be the most appropriate for most applications. The system met the main standards in the NHSBSP and European protocols and is suitable for evaluation at a clinical site in the NHSBSP.

REFERENCES

1. Workman A, Castellano I, Kulama E, et al. *Commissioning and Routine Testing of Full Field Digital Mammography Systems*, version 3. NHS Cancer Screening Programmes, 2009 (NHSBSP Equipment Report 0604).
2. Young KC, Johnson B, Bosmans H, Van Engen R. Development of minimum standards for image quality and dose in digital mammography. In: *Digital Mammography, Proceedings of the 7th International Workshop on Digital Mammography*, Durham NC, USA, June 2004 (2005).
3. Van Engen R, Young KC, Bosmans H, Thijssen M. The European protocol for the quality control of the physical and technical aspects of mammography screening. Part B: Digital mammography. In: *European Guidelines for Quality Assurance in Breast Cancer Screening and Diagnosis*, 4th edn. Luxembourg: European Commission, 2006: 732–739.
4. Young KC, Cook JJH, Oduko JM, Bosmans H. Comparison of software and human observers in reading images of the CDMAM test object to assess digital mammography systems. *Proceedings of SPIE Medical Imaging*, 2006, 614206: 1–13.
5. Young KC, Cook JJH, Oduko JM. Automated and human determination of threshold contrast for digital mammography systems. In: Astley SM, Bradey M, Rose C, Zwigelaar R, eds. *Proceedings of the 8th International Workshop on Digital Mammography. Lecture Notes in Computer Science*, 2006, 4046: 266–272.
6. Young KC, Alsager A, Oduko JM, et al. Evaluation of software for reading images of the CDMAM test object to assess digital mammography systems. *Proceedings of SPIE Medical Imaging*, 2008, 69131C: 1–11.
7. Young KC, Oduko JM. *Evaluation of Kodak DirectView Mammography Computerised Radiography*. NHS Cancer Screening Programmes, 2005 (NHSBSP Equipment Report 0504).
8. Young KC, Oduko JM, Woolley L. *Technical Evaluation of the Hologic Selenia Full Field Digital Mammography System*. NHS Cancer Screening Programmes, 2007 (NHSBSP Equipment Report 0701).
9. Young KC, Oduko JM. *Technical Evaluation of Kodak DirectView Mammography Computerised Radiography System using EHR-M2 Plates*. NHS Cancer Screening Programmes, 2007 (NHSBSP Equipment Report 0706).
10. Young KC, Oduko JM. *Technical Evaluation of Agfa CR-85 Mammography System*. NHS Cancer Screening Programmes, 2007 (NHSBSP Equipment Report 0707).
11. Young KC, Oduko JM. *Technical Evaluation of the Hologic Selenia Full Field Digital Mammography System with a Tungsten Tube*. NHS Cancer Screening Programmes, 2008 (NHSBSP Equipment Report 0801).
12. Young KC, Oduko JM, Gundogdu O, Alsager A. *Technical Evaluation of the GE Essential Full Field Digital Mammography System*. NHS Cancer Screening Programmes, 2008 (NHSBSP Equipment Report 0803).
13. Oduko JM, Young KC, Alsager A, Gundogdu O. *Technical Evaluation of the IMS Giotto Full Field Digital Mammography System with a Tungsten Tube*. NHS Cancer Screening Programmes, 2008 (NHSBSP Equipment Report 0804).
14. Young KC, Oduko JM, Alsager A. *Technical Evaluation of the Sectra MDM-L30 Full Field Digital Mammography System*. NHS Cancer Screening Programmes, 2008 (NHSBSP Equipment Report 0805).
15. Young KC, Oduko JM, Alsager A. *Technical Evaluation of the Konica Minolta Regius 190 CR Mammography System and Three Types of Image Plate*. NHS Cancer Screening Programmes, 2008 (NHSBSP Equipment Report 0806).
16. Young KC, Oduko JM, Gundogdu O, Asad M. *Technical Evaluation of Profile Automatic Exposure Control Software on GE Essential Full Field Digital Mammography Systems*. NHS Cancer Screening Programmes, 2009 (NHSBSP Equipment Report 0903)].

